Supporting Information

Reactivity of Proton Sources with a Nickel Hydride Complex in Acetonitrile: Implications for the Study of Fuel-Forming Catalysts

*Eric S. Rountree and Jillian L. Dempsey**

Department of Chemistry, University of North Carolina
Chapel Hill, North Carolina 27599-3290, United States
**email: dempseyj@email.unc.edu*

Table of Contents *Page*

SI–1 Determination of acid pK_a for previously unknown acids

4-methylanilinium tetrafluoroborate

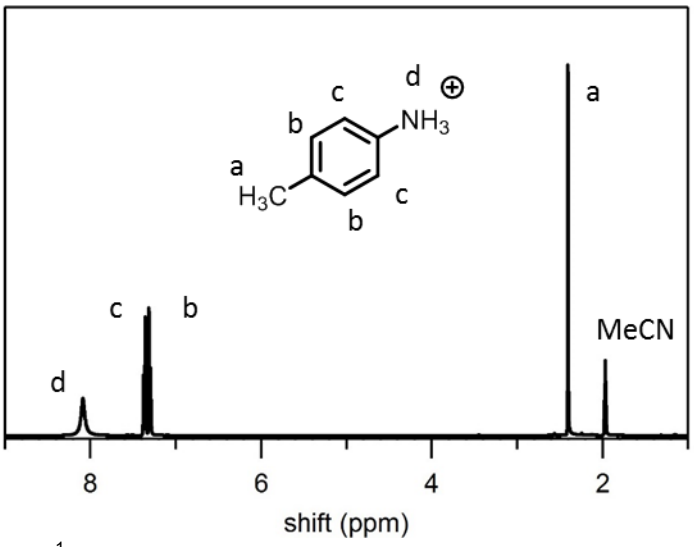

Figure S1. ^{1}H NMR of 4-methylanilinium tetrafluoroborate in CD_3CN.

The pK_a of 4-methylanilinium in acetonitrile was determined via spectrophotometric titration as previously described.[1] 4-methylanilinum was titrated into a solution of methyl orange (MO, pK_a = 10.6) and the protonated methyl orange (MOH^+) absorbance was monitored by UV-vis absorbance spectroscopy at λ = 550 nm (ε = 38,650 $cm^{-1}M^{-1}$). Concentrations of 4-methylanilinium, 4-methylaniline, and methyl orange at each titration point were calculated based on the concentration protonated methyl orange (determined by UV-vis) and the initial concentrations of all reagents. Linear regression of a plot of ([4-CH_3-aniline]/[4-CH_3-anilinium][MOH^+] was used to determine the pK_a of 4-methylanilnium: $pK_a = pK_a(methyl\ orange) - \log(slope)$.

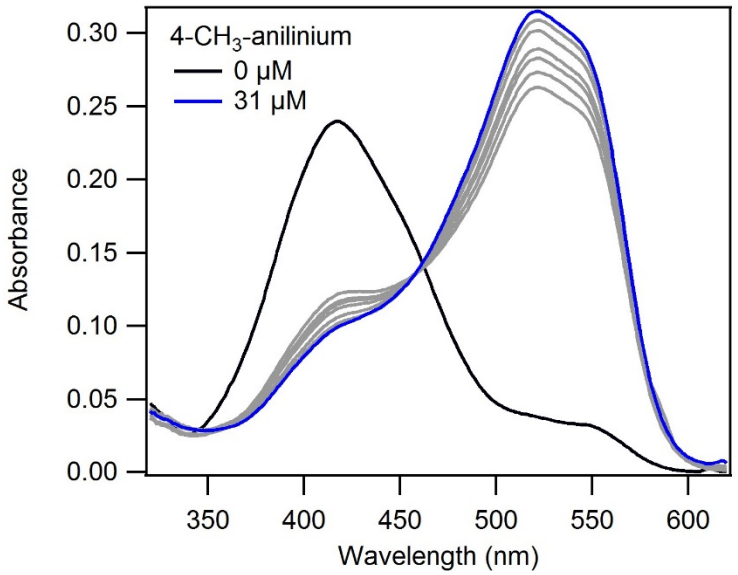

Figure S2. Spectrophotometric titration of 11 μM methyl orange with 4-methylanilinium. Above 350 nm, the 4-methylanilinium extinction coefficient does not exceed 0.4 $cm^{-1}M^{-1}$, four orders of magnitude less than methyl orange and protonated methyl orange and therefore does not contribute significantly to the overall absorbance signal.

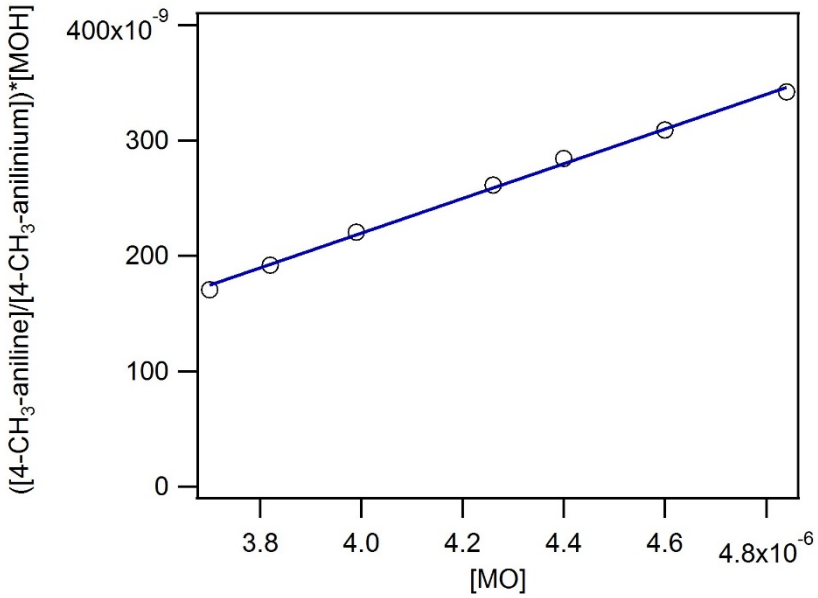

Figure S3. The slope of ([4-CH_3-aniline]/[4-CH_3-anilinium])[MOH] versus [MO] (m = 0.15) can be used to determine the pK_a for 4-methylanilinium (pK_a = 11.4). R^2 = 0.997.

4-iodoanilinium tetrafluoroborate

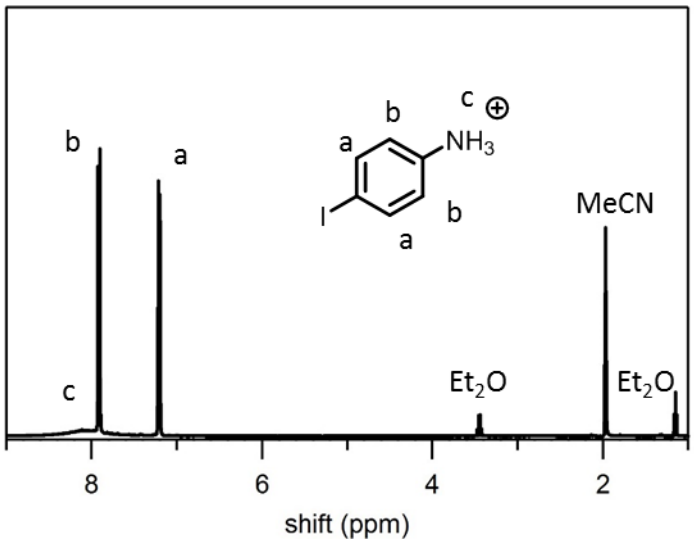

Figure S4. ^{1}H NMR of 4-iodoanilinium tetrafluoroborate in CD_3CN.

To determine the pK_a of 4-iodoanilinium, a spectrophotometric titration was performed following the same procedure as described for 4-methylanilinium, except that 3-nitroaniline was used as the indicator (pK_a = 7.68), and there was a minor contribution from the 4-iodoanilinium absorbance that had to be subtracted out.

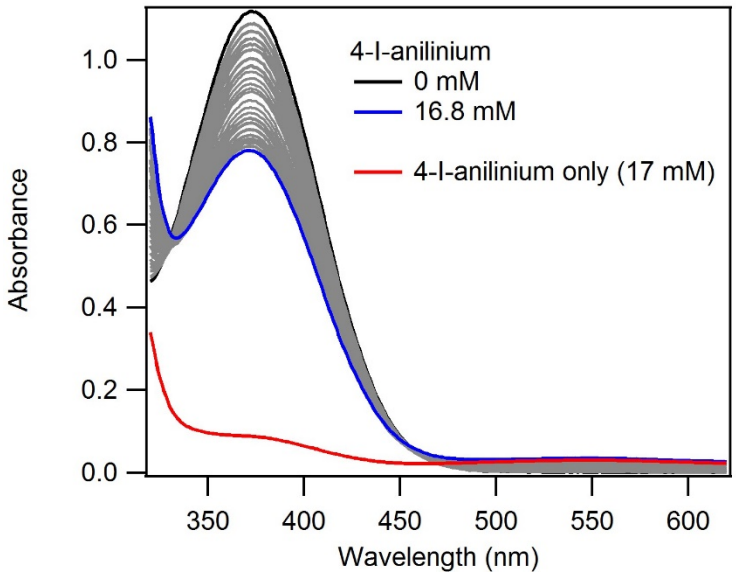

Figure S5. Spectrophotometric titration of 0.865 mM 3-nitroaniline with 4-iodoanilinium. The absorbance for 4-iodoanilinium is shown in red. This contribution to the overall absorbance signal was subtracted out (proportional to its concentration) in the making of Figure S6 to determine the pK_a of 4-iodoanilinium.

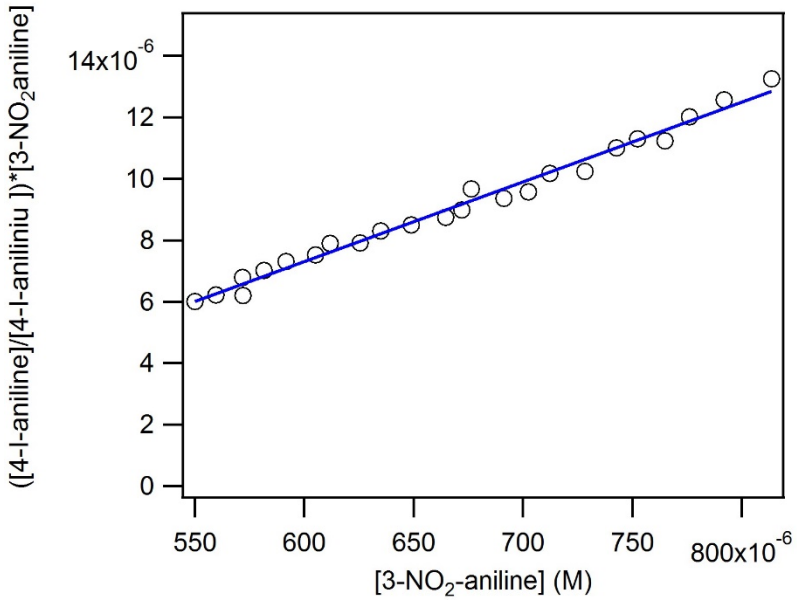

Figure S6. The slope of ([4-I-aniline]/[4- I-anilinium])*[3-NO_2-anilium] versus [3-NO_2-aniline] (m = 0.025966) can be used to determine the pK_a for 4-iodoanilinium (pK_a = 9.27). R^2 = 0.986.

SI–2 Data for Figure 1

Table S1. pK_a values of *para*-substituted anilinium derivatives in acetonitrile, rate constants for reaction with $Ni^{II}H$

Acid	*para*-substituent	pK_a	Reference	k ($M^{-1}s^{-1}$)
4-methoxyanilinium	$-OCH_3$	11.86	2	7
4-methylanilinium	$-CH_3$	11.4	this work	15.8
4-tertbutylanilinium	$-C(CH_3)_3$	11.1	1	16.2
anilinium	n/a	10.62	2	58 (Ref. 3)
4-chloroanilinium	–Cl	9.7	1	194
4-bromoanilinium	-Br	9.43	1	220
4-trifluoromethoxyanilinium	$-OCF_3$	9.28	4	199
4-iodoanilinium	-I	9/27	this work	220
4-(methylbenzoate)anilinium	$-COOCH_3$	8.62	4	553
4-trifluoromethylanilinium	$-CF_3$	8.03	2	538
4-cyanoanilinium	-CN	7.0	1	762

Stopped flow kinetics traces and observed rate constant versus concentration data for each acid

4-methoxyanilinium

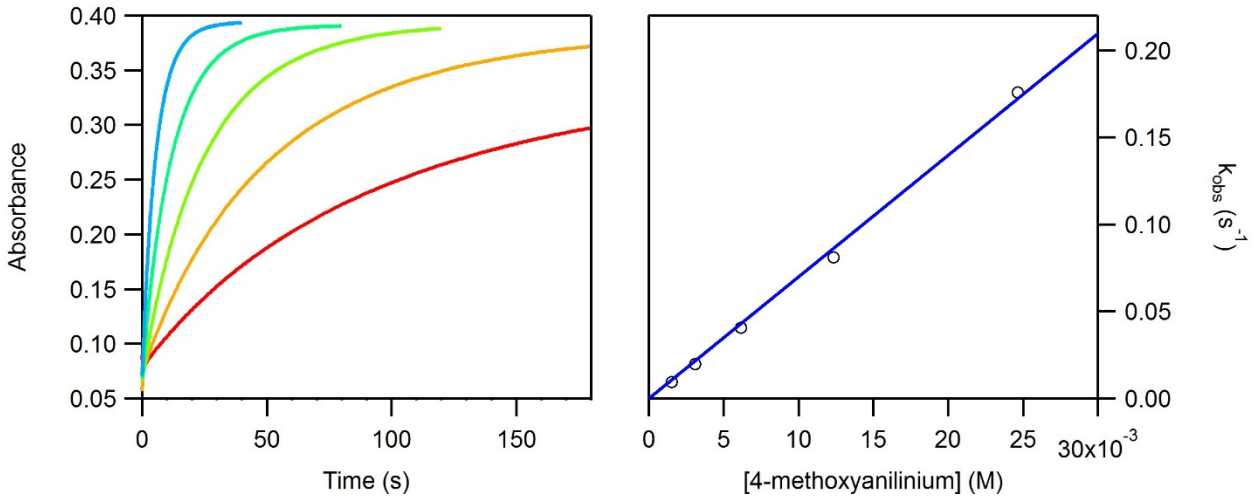

Figure S7. Left: Stopped-flow kinetics traces for the reaction of $Ni^{II}H$ with various concentrations of 4-(methoxy)anilinium to generate H_2 and Ni^{II} (λ_{obs} = 500 nm). Right: Observed rate constant obtained from kinetics traces plotted vs. acid concentration. Blue line (slope = 7 $M^{-1}s^{-1}$, R^2 = 0.997) represents the fit of the data with the intercept fixed at the origin.

4-methylanilinium

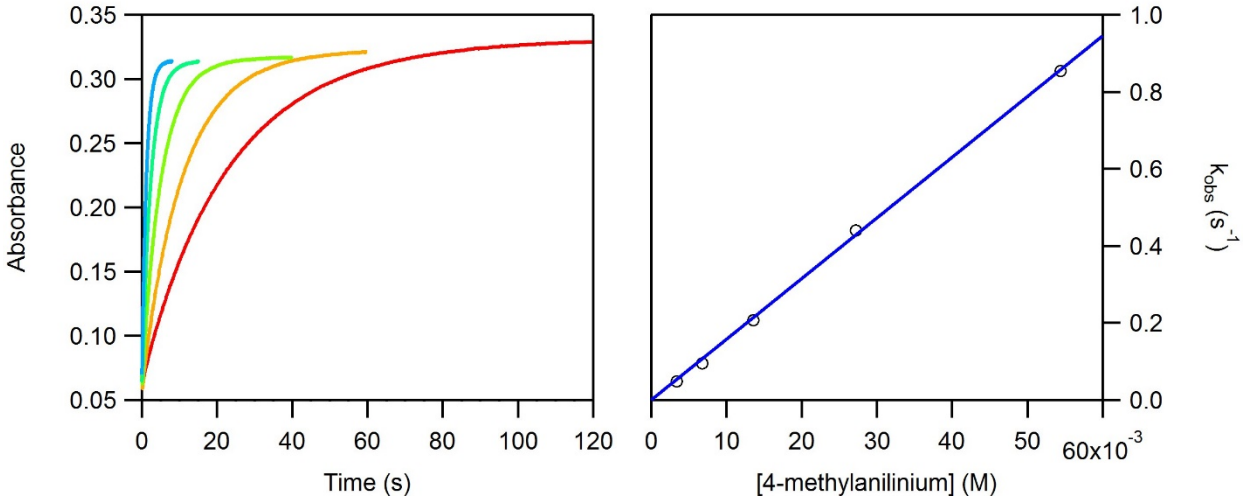

Figure S8. Left: Stopped-flow kinetics traces for the reaction of $Ni^{II}H$ with various concentrations of 4-methylanilinium to generate H_2 and Ni^{II} (λ_{obs} = 500 nm). Right: Observed rate constant obtained from kinetics traces plotted vs. acid concentration. Blue line (slope = 15.8 $M^{-1}s^{-1}$, R^2 = 0.999) represents the fit of the data with the intercept fixed at the origin.

4-tertbutylanilinium

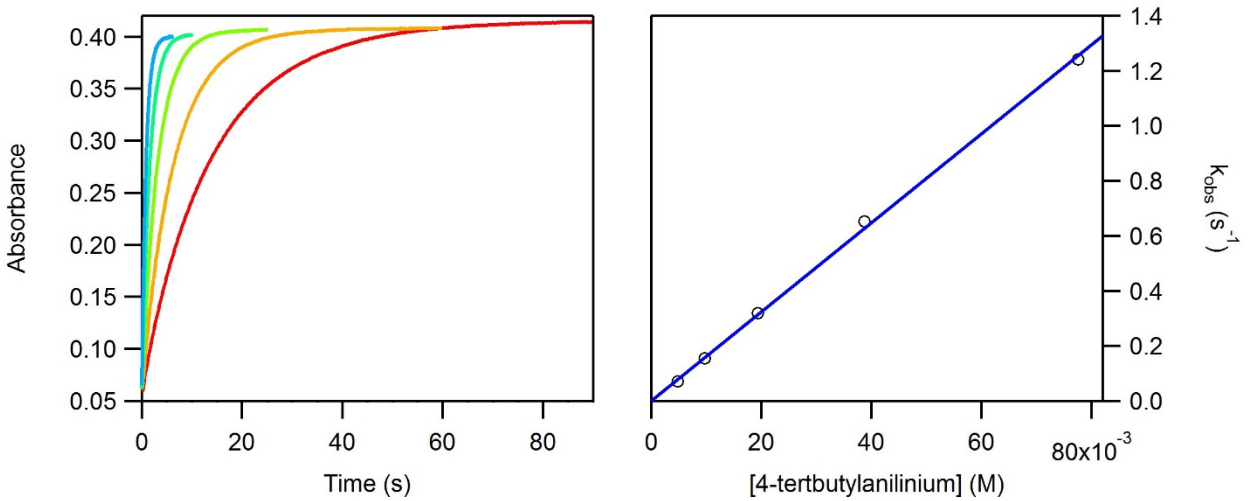

Figure S9. Left: Stopped-flow kinetics traces for the reaction of $Ni^{II}H$ with various concentrations of 4-tertbutylanilinium to generate H_2 and Ni^{II} (λ_{obs} = 500 nm). Right: Observed rate constant obtained from kinetics traces plotted vs. acid concentration. Blue line (slope = 16.2 $M^{-1}s^{-1}$, R^2 = 0.999) represents the fit of the data with the intercept fixed at the origin.

4-chloroanilinium

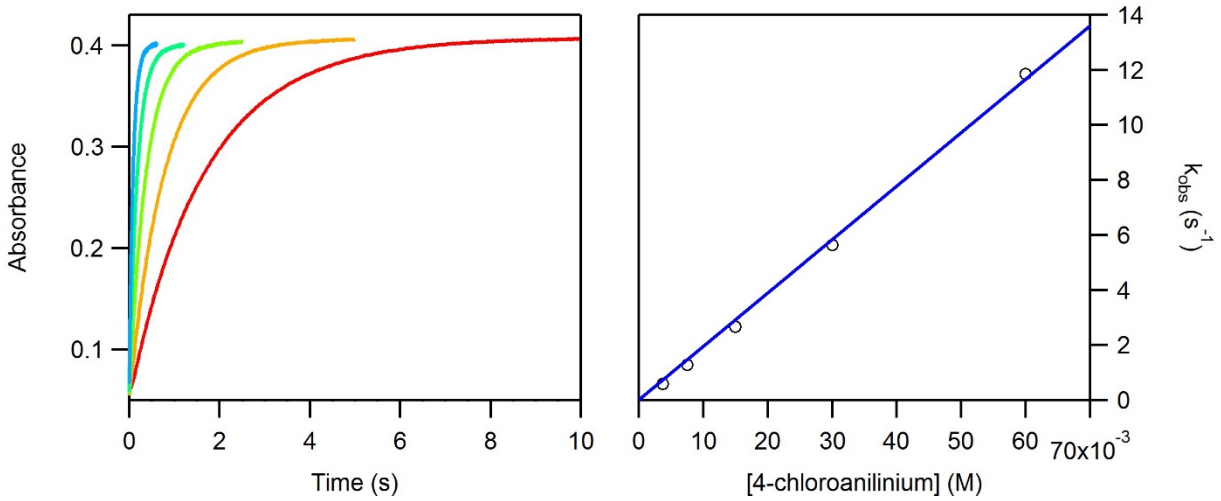

Figure S10. Left: Stopped-flow kinetics traces for the reaction of $Ni^{II}H$ with various concentrations of 4-chloroanilinium to generate H_2 and Ni^{II} (λ_{obs} = 500 nm). Right: Observed rate constant obtained from kinetics traces plotted vs. acid concentration. Blue line (slope = 194 $M^{-1}s^{-1}$, R^2 = 0.998) represents the fit of the data with the intercept fixed at the origin.

4-bromoanilinium

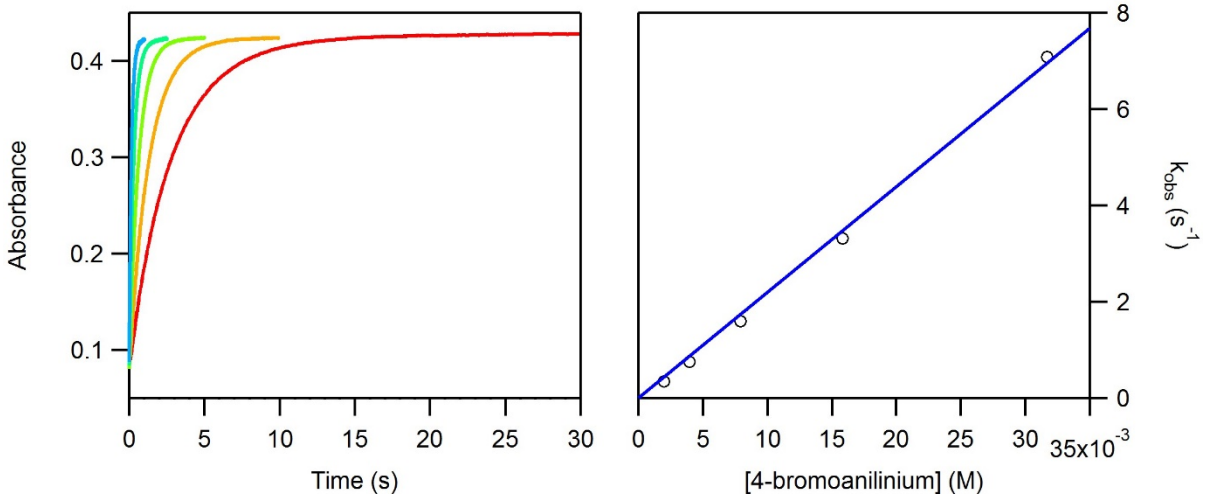

Figure S11. Left: Stopped-flow kinetics traces for the reaction of $Ni^{II}H$ with various concentrations of 4-bromoanilinium to generate H_2 and Ni^{II} (λ_{obs} = 500 nm). Right: Observed rate constant obtained from kinetics traces plotted vs. acid concentration. Blue line (slope = 220 $M^{-1}s^{-1}$, R^2 = 0.997) represents the fit of the data with the intercept fixed at the origin.

4-trifluoromethoxyanilinium

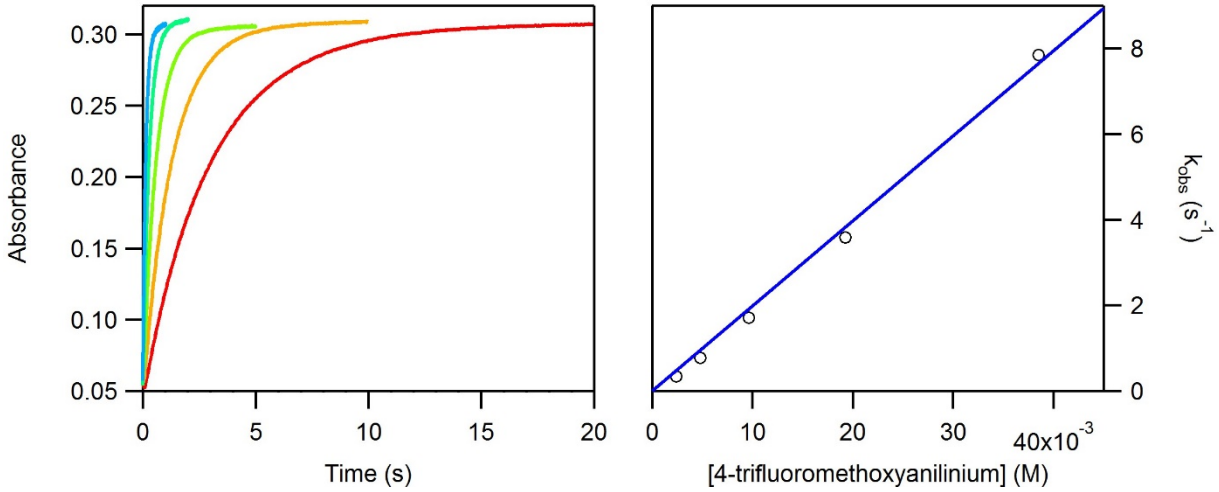

Figure S12. Left: Stopped-flow kinetics traces for the reaction of $Ni^{II}H$ with various concentrations of 4-trifluoromethoxyanilinium to generate H_2 and Ni^{II} (λ_{obs} = 500 nm). Right: Observed rate constant obtained from kinetics traces plotted vs. acid concentration. Blue line (slope = 199 $M^{-1}s^{-1}$ R^2 = 0.995) represents the fit of the data with the intercept fixed at the origin.

4-iodoanilinium

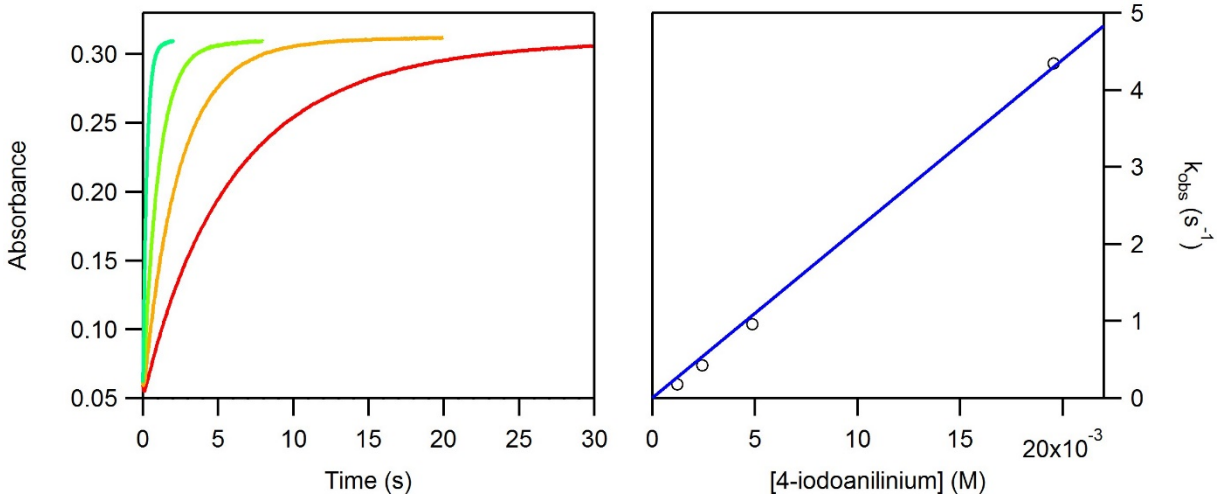

Figure S13. Left: Stopped-flow kinetics traces for the reaction of $Ni^{II}H$ with various concentrations of 4-iodoanilinium to generate H_2 and Ni^{II} (λ_{obs} = 500 nm). Right: Observed rate constant obtained from kinetics traces plotted vs. acid concentration. Blue line (slope = 220 $M^{-1}s^{-1}$, R^2 = 0.997) represents the fit of the data with the intercept fixed at the origin.

4-(methylbenzoate)anilinium

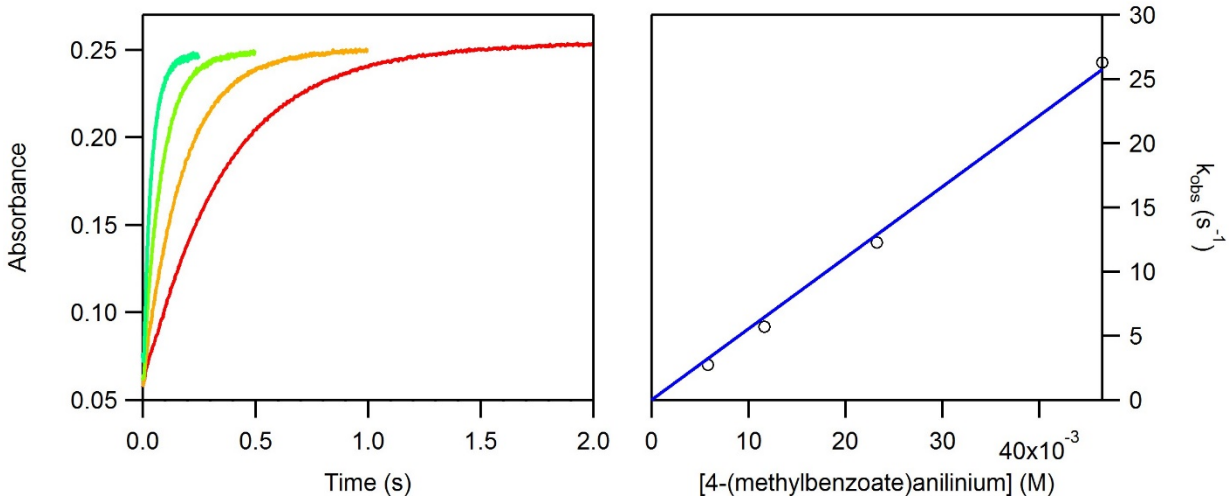

Figure S14. Left: Stopped-flow kinetics traces for the reaction of $Ni^{II}H$ with various concentrations of 4-(methylbenzoate)anilinium to generate H_2 and Ni^{II} (λ_{obs} = 500 nm). Right: Observed rate constant obtained from kinetics traces plotted vs. acid concentration. Blue line (slope = 553 $M^{-1}s^{-1}$, R^2 = 0.996) represents the fit of the data with the intercept fixed at the origin.

4-trifluoromethylanilinium

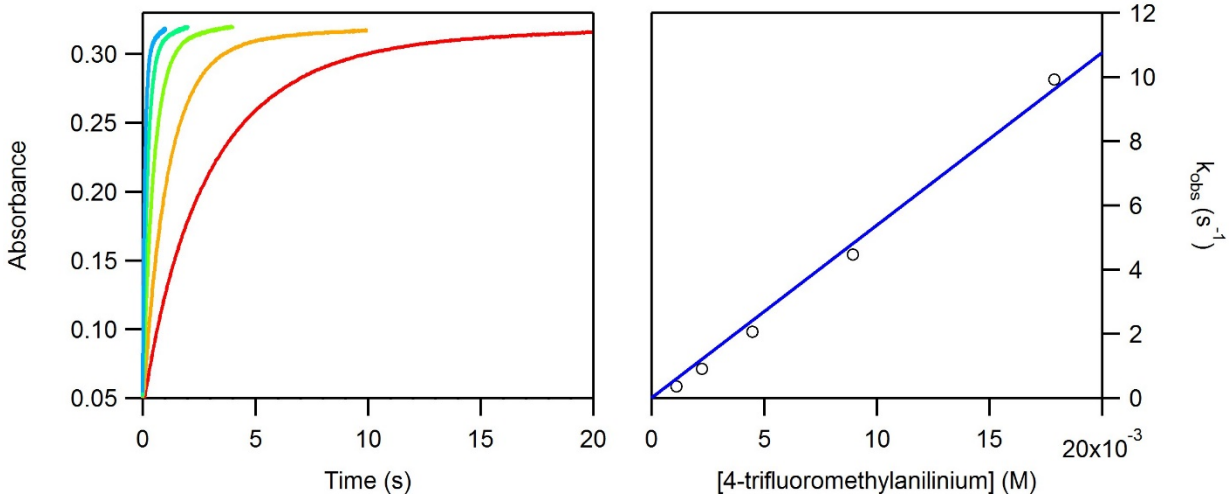

Figure S15. Left: Stopped-flow kinetics traces for the reaction of $Ni^{II}H$ with various concentrations of 4-trifluoromethylanilinium to generate H_2 and Ni^{II} (λ_{obs} = 500 nm). Right: Observed rate constant obtained from kinetics traces plotted vs. acid concentration. Blue line (slope = 538 $M^{-1}s^{-1}$, R^2 = 0.997) represents the fit of the data with the intercept fixed at the origin.

4-cyanoanilinium

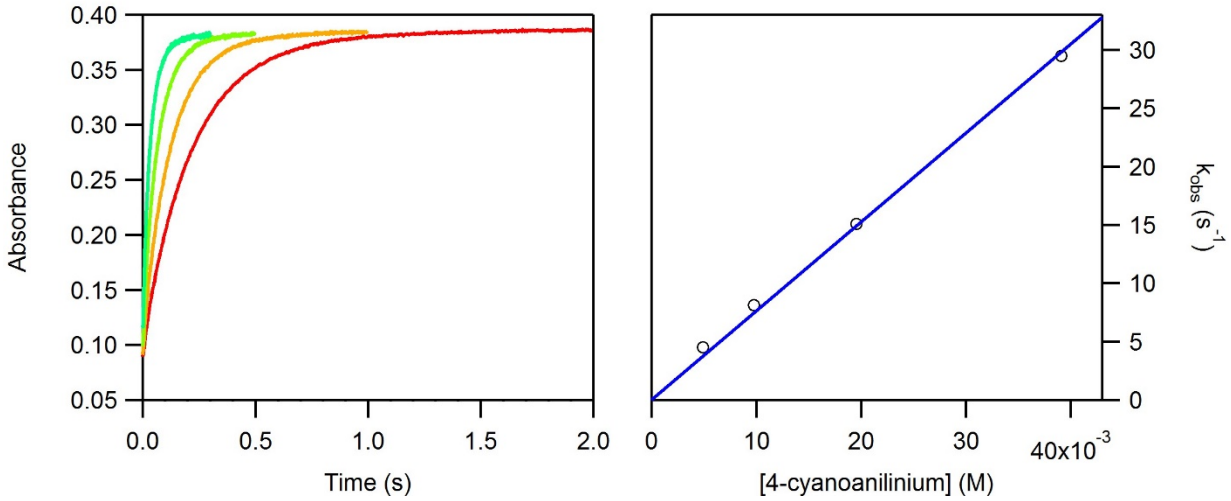

Figure S16. Left: Stopped-flow kinetics traces for the reaction of $Ni^{II}H$ with various concentrations of 4-cyanoanilinium to generate H_2 and Ni^{II} (λ_{obs} = 500 nm). Right: Observed rate constant obtained from kinetics traces plotted vs. acid concentration. Blue line (slope = 762 M^{-1} s^{-1}, R^2 = 0.997) represents the fit of the data with the intercept fixed at the origin.

Hammett Plot

As discussed in the main text, the data in Figure 1 can also be displayed in a Hammett format. We accomplish this using the σ_P values of the para-substituents from the literature[5] for the horizontal axis and log(K/K_H) for the vertical axis. Because σ_P and pK_a are related values, Figure 1 and Figure S17 are very similar in appearance and the same information can be inferred from each.

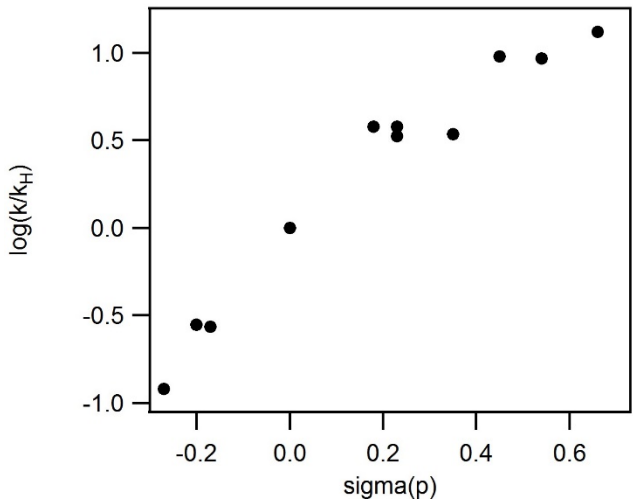

Figure S17. Hammett plot derived from the rate constants reported in Table S1.

SI–3 Base:Acid Ratios

Stopped flow kinetics traces and observed rate versus [base] data for each acid

tetrabutylammonium trifluoroacetate: trifluoroacetic acid

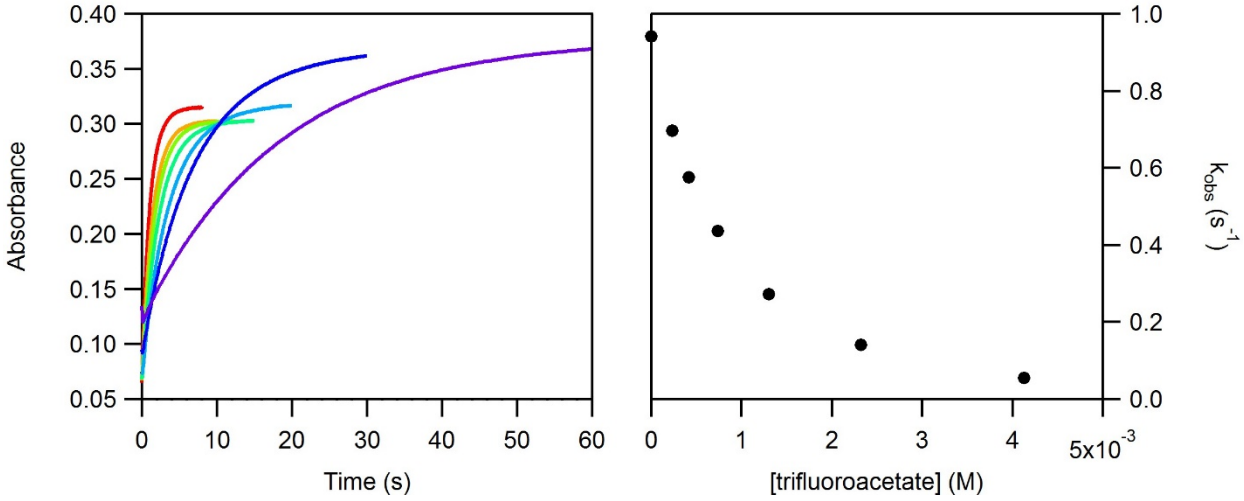

Figure S18. Left: Stopped-flow kinetics traces for the reaction of $Ni^{II}H$ with various ratios of trifluoroacetate:trifluoroacetic acid to generate H_2 and Ni^{II} (λ_{obs} = 500 nm). The shift in absorbance for the slower datasets (higher base concentration), appeared to arise from the formation of some precipitate upon mixing. This was only seen with TFA. Right: Observed rate constant obtained from kinetics traces plotted against base concentration. Trifluoroacetic acid concentration was fixed at 9.5 mM, trifluoroacetate varied.

4-methylaniline:4-methylanilinium tetrafluoroborate

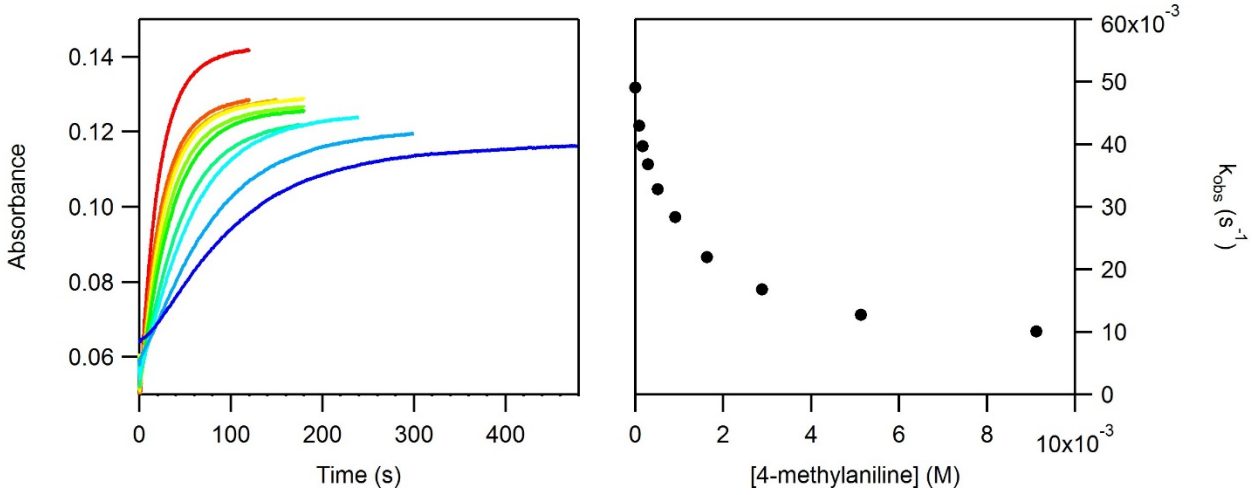

Figure S19. Left: Stopped-flow kinetics traces for the reaction of $Ni^{II}H$ with various ratios of 4-methylaniline:4-methylanilinium to generate H_2 and Ni^{II} (λ_{obs} = 500 nm). The decrease in final absorbance as base concentration is increased is a result of equilibrium formation as Ni^{II} can split H_2 in the presence of a strong base. Right: Observed rate constant obtained from kinetics traces plotted against base concentration. 4-methylanilinium concentration was fixed at 6.77 mM, base was varied.

Aniline:anilinium tetrafluoroborate

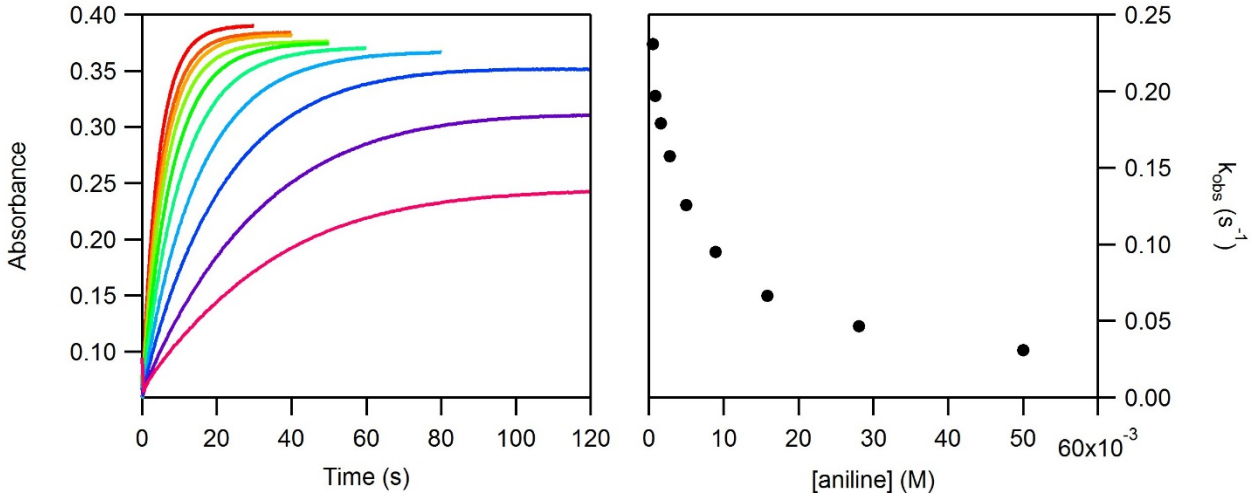

Figure S20. Left: Stopped-flow kinetics traces for the reaction of $Ni^{II}H$ with various ratios of aniline:anilinium to generate H_2 and Ni^{II} (λ_{obs} = 500 nm). The decrease in final absorbance as base concentration is increased is a result of equilibrium formation as Ni^{II} can split H_2 in the presence of a strong base. Right: Observed rate constant obtained from kinetics traces plotted against base concentration. Anilinium concentration was fixed at 5 mM, base was varied.

4-bromoaniline:4-bromoanilinium tetrafluoroborate

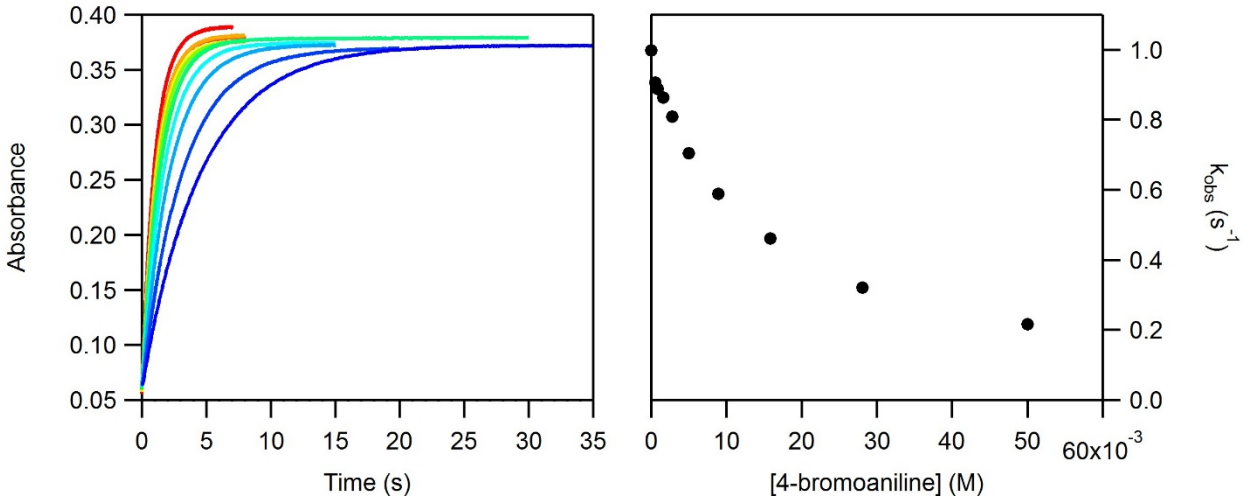

Figure S21. Left: Stopped-flow kinetics traces for the reaction of $Ni^{II}H$ with various ratios of 4-bromoaniline:4-bromoanilinium to generate H_2 and Ni^{II} (λ_{obs} = 500 nm).Right: Observed rate constant obtained from kinetics traces plotted against base concentration. 4-bromoanilinium concentration was fixed at 5 mM, base was varied.

4-(methylbenzoate)aniline:4-(methylbenzoate)anilinium tetrafluoroborate

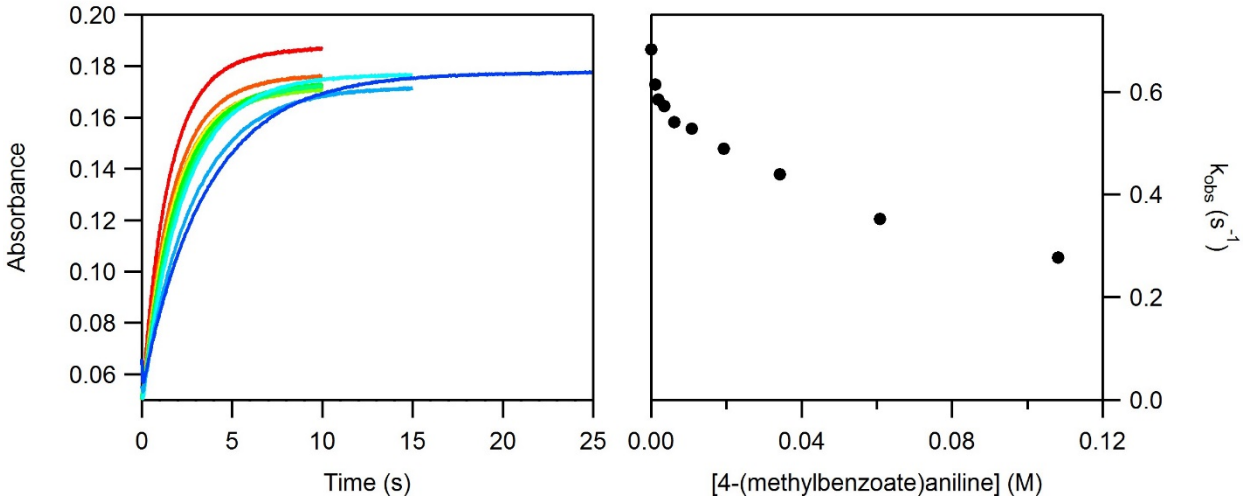

Figure S22. Left: Stopped-flow kinetics traces for the reaction of $Ni^{II}H$ with various ratios of 4-(methylbenzoate)aniline:4--(methylbenzoate)anilinium to generate H_2 and Ni^{II} (λ_{obs} = 500 nm).Right: Observed rate constant obtained from kinetics traces plotted against base concentration. 4--(methylbenzoate)anilinium concentration was fixed at 1.6 mM, base was varied.

4-trifluoromethylaniline:4-trifluoromethylanilinium tetrafluoroborate

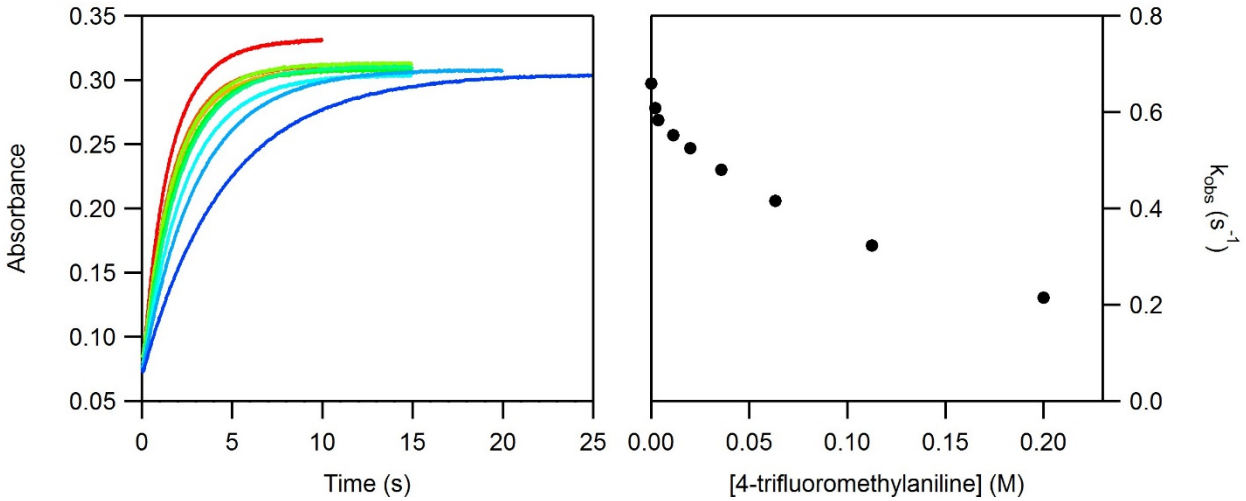

Figure S23. Left: Stopped-flow kinetics traces for the reaction of $Ni^{II}H$ with various ratios of 4-trifluoromethylaniline:4-trifluoromethylanilinium to generate H_2 and Ni^{II} (λ_{obs} = 500 nm).Right: Observed rate constant obtained from kinetics traces plotted against base concentration. 4-trifluoromethylanilinium concentration was fixed at 3.1 mM, base was varied.

4-cyanoaniline:4-cyanoanilinium tetrafluoroborate

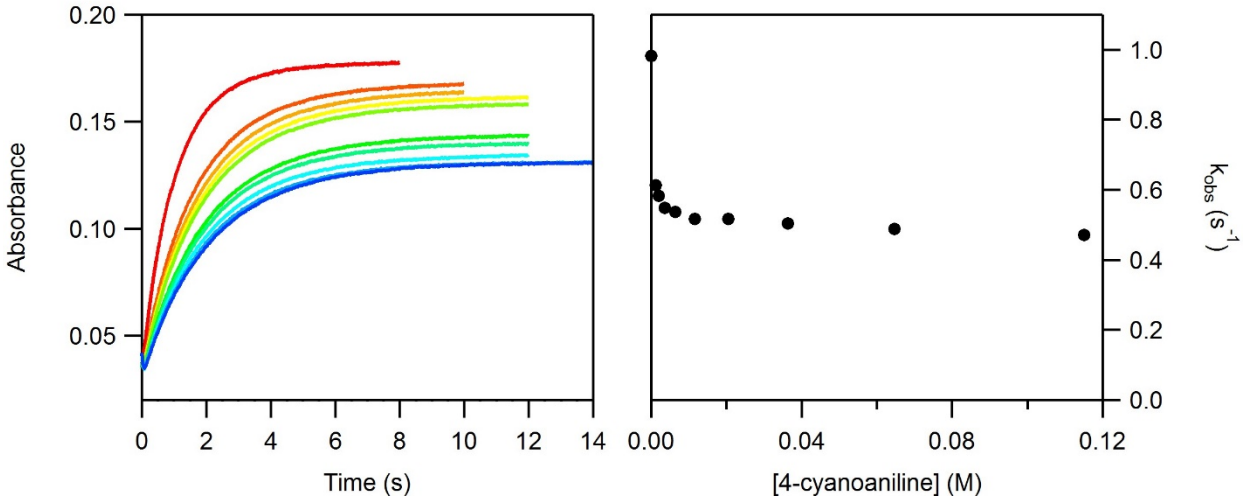

Figure S24. Left: Stopped-flow kinetics traces for the reaction of $Ni^{II}H$ with various ratios of 4-cyanoaniline:4-cyanoanilinium to generate H_2 and Ni^{II} (λ_{obs} = 500 nm).Right: Observed rate constant obtained from kinetics traces plotted against base concentration. 4-cyanoanilinium concentration was fixed at 1 mM, base was varied.

dimethylformamide:dimethylformamidium triflate

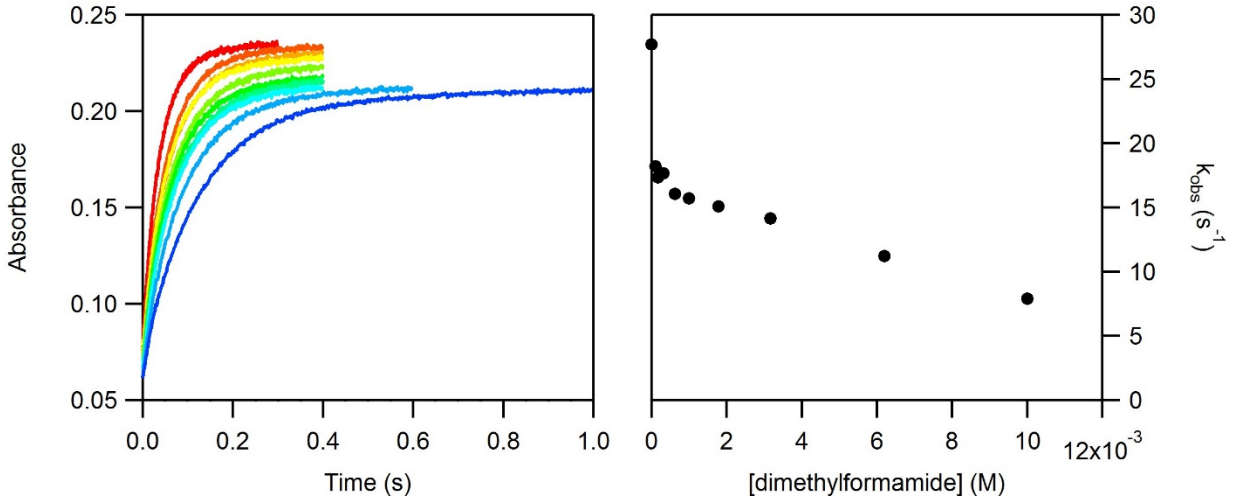

Figure S25. Left: Stopped-flow kinetics traces for the reaction of $Ni^{II}H$ with various ratios of dimethylformamide:dimethylfomamidium to generate H_2 and Ni^{II} (λ_{obs} = 500 nm).Right: Observed rate constant obtained from kinetics traces plotted against base concentration. dimethylformamidium concentration was fixed at 1 mM, base was varied.

Figure containing all datasets

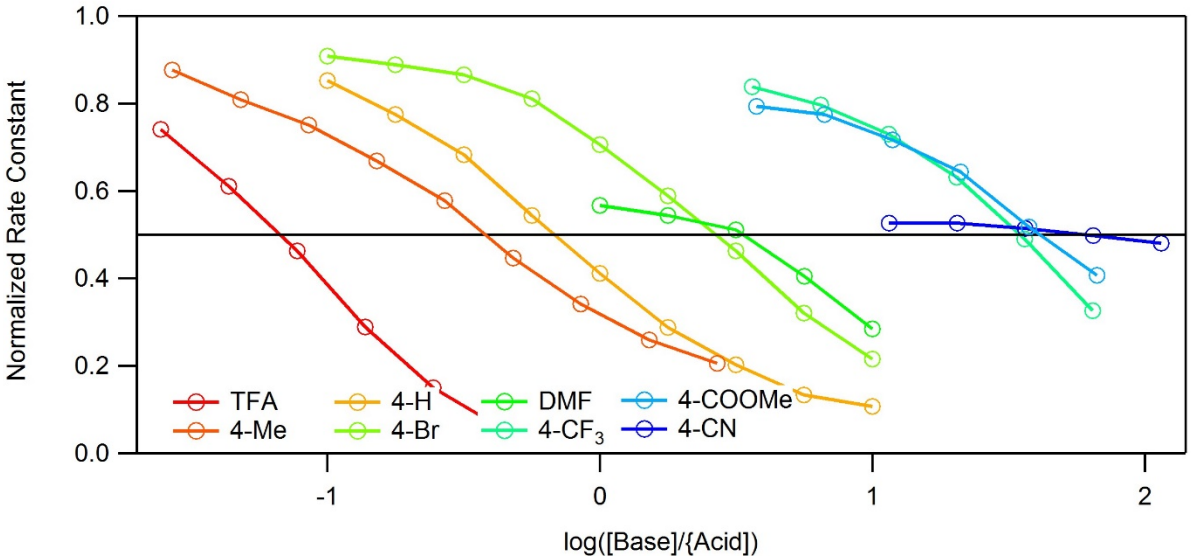

Figure S26. Normalized rate constant plotted vs. base:acid ratio. Observed first order rate constants determined in the presence of base were normalized to the observed first order rate constant in the absence of base. In each case, the acid concentration was held constant and the base concentration was varied. Trifluoroacetic acid (TFA, pK_a = 12.65, 9.5 mM), 4-methylanilinium (4-Me, pK_a = 11.4, 3.4 mM), anilinium (4-H, pK_a = 10.62, 5 mM), and 4-bromoanilinium (4-Br, pK_a = 9.43, 5 mM), dimethylformamidium (DMF, pK_a =6.1, 1 mM), 4-trifluoromethylanilinium (4-CF_3, pK_a = 8.03, 3.1 mM),, 4-(methylbenzoate)anilinium (4-COOMe, pK_a = 8.6, 1.6 mM),, and 4-cyanoanilinium (4-CN, pK_a = 7, 1 mM), are represented here. The acids with a pK_a values lower than 9 did not follow any trend, in keeping the pK_a independence shown for this range in Figure 1. Markers represent actual data points; lines in between are a guide for the eye.

SI–4 Homoconjugation

Determination of the homoconjugation constant for 4-cyanoanilinium

^{1}H NMR was used to determine the homoconjugation constant for 4-cyanoanlinium. In the case that a proton is rapidly exchanging between multiple locations, only one peak will appear. The shift of that peak is dependent upon the shift of each pure species and the percentage of protons in each state. For 4-cyanoanilinium, this is represented as equation S1, where δ is the observed shift, $\%H_X$ is the percentage of protons in state X, δ_X is the shift for pure X. For 4-cyanoanilinium, there are three possible states, B (4-cyanoaniline), BH (4-cyanonanilinium), and BHB (homoconjugated species).

$$\delta = \%H_B\delta_B + \%H_{BH}\delta_{BH} + \%H_{BHB}\delta_{BHB} \quad (S1)$$

Because each of the species present contains a different number of protons participating in the exchange process, we have to account for this using equation S2, where n represents the number of exchanging protons on species X and χ_X represents the mole fraction of species X.

$$\%H_X = \frac{n\chi_X}{2\chi_B + 3\chi_{BH} + 5\chi_{BHB}} \quad (S2)$$

$$\delta = \frac{2\chi_B\delta_B + 3\chi_{BH}\delta_{BH} + 5\chi_{BHB}\delta_{BHB}}{2\chi_B + 3\chi_{BH} + 5\chi_{BHB}} \quad (S3)$$

To relate equation S3 to the homoconjugation constant, we must solve for the concentration of the homoconjugated species in the equilibrium equation. As is explained below in the experiment description, we simplified our analysis by using a 1:1 ratio of B and BH and then varied the total concentration. Thus, we simplify the input concentration of B and BH to be represented as $[I]_0$

$$[I]_0 = [B]_0 = [BH]_0 \quad (S4)$$

$$K = \frac{[BHB]}{[B][BH]} = \frac{[BHB]}{([I]_0 - [BHB])^2} \quad (S5)$$

$$[BHB] = [I]_0 + \frac{1 - \sqrt{1 + 4K[I]_0}}{2K} \quad (S6)$$

$$\chi_B = \chi_{BH} = \frac{([I]_0 - [BHB])}{2([I]_0 - [BHB]) + [BHB]} = \frac{([I]_0 - [BHB])}{2[I]_0 - [BHB]} \quad (S7)$$

$$\chi_{BHB} = \frac{[BHB]}{2([I]_0 - [BHB]) + [BHB]} = \frac{[BHB]}{2[I]_0 - [BHB]} \quad (S8)$$

Substituting S7 and S8 into S3 results in:

$$\delta = \frac{2([I]_0 - [BHB])\delta_B + 3([I]_0 - [BHB])\delta_{BH} + 5[BHB]\delta_{BHB}}{5[I]_0} \quad (S9)$$

Equation S9 can be further simplified by acknowledging that δ_B and δ_{BH} can be represented as a single parameter, δ_I.

$$\delta_I = \frac{2}{5}\delta_B + \frac{3}{5}\delta_{BH} \quad (S10)$$

$$\delta = \frac{([I]_0 - [BHB])}{[I]_0}\delta_I + \frac{[BHB]}{[I]_0}\delta_{BHB} \quad (S11)$$

Substituting in S6 into S11 we obtain our fitting equation for our NMR shift, with three dependent variables K, δ_I, and δ_{BHB}.

$$\delta = \frac{\sqrt{1 + 4K[I]_0} - 1}{2K[I]_0}\delta_I + \left(1 + \frac{1 - \sqrt{1 + 4K[I]_0}}{2K[I]_0}\right)\delta_{BHB} \quad (S12)$$

The homoconjugation constant was therefore determined by the average of three separate experiments. Each experiment followed a generic procedure in which 1 mL of a deuterated acetonitrile stock solution of 1:1 4-cyanoaniline:4-cyanoanilinium was prepared in an inert atmosphere glovebox. To three separate J-Young tubes, 0.125 mL, 0.25 mL, and 0.5 mL of stock solution were added. Each was then diluted to 0.5 mL total. After taking NMRs, the solutions were each then diluted by 0.1 mL. This was repeated 5-6 times to complete a dataset. After referencing the proteo-impurity of acetonitrile to 1.94 ppm,[6] the peak location of the acidic protons was recorded. After plotting the chemical shift against the input concentration, $[I]_0$, the datasets were fit using equation S12 (Figure S27).

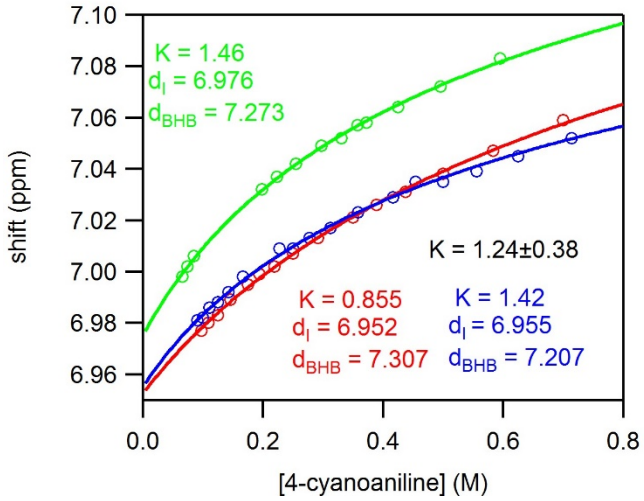

Figure S27. Three titrations of 1:1 mixtures of 4-cyanoaniline:4-cyanoanilinium in deuterated acetonitrile. The fits represent equations S12. The average value for K from the three datasets was 1.24 ± 0.38 M^{-1}.

Tosic Acid Kinetic Trace

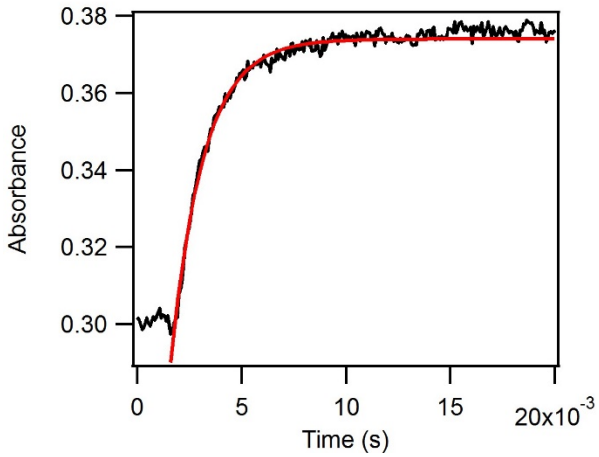

Figure S28. Stopped-flow kinetics trace for the reaction of $Ni^{II}H$ with 5 mM of tosic acid to generate H_2 and Ni^{II} (λ_{obs} = 500 nm). Fit, shown in red, gives an observed rate constant of 640 s^{-1}.

SI–5 Acid Concentration Independence

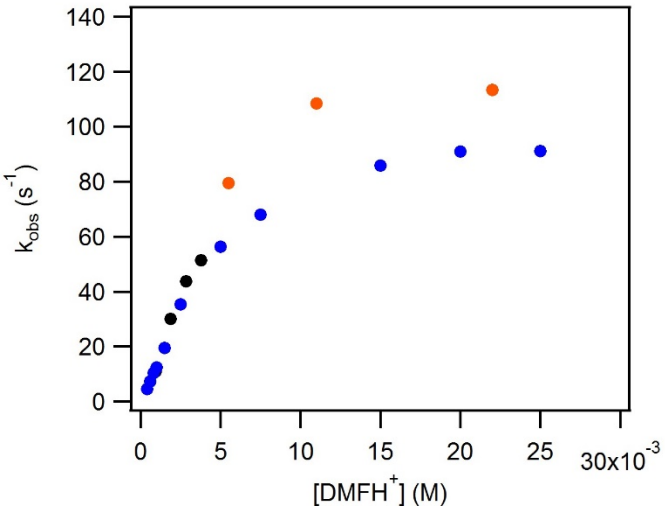

Figure S29. Observed rate constant plotted against dimethylformamidium concentration; rate data obtained from stopped-flow kinetics traces monitoring the appearance Ni^{II} (λ_{obs} = 500 nm). The colored data points represent separate experiments. While the observed rate constant always plateaued around 10 mM $DMFH^+$, the rate constant at which it plateaued at was inconsistent.

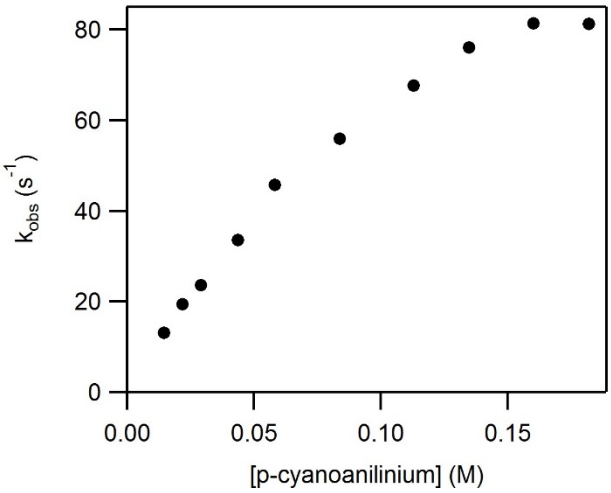

Figure S30. Observed rate constant plotted against p-cyanoanilinium concentration; rate data obtained from stopped-flow kinetics traces monitoring the appearance of Ni^{II} (λ_{obs} = 500 nm).

SI–6 Water in acetonitrile

Water addition to anilinium

Figure 5 in the main text shows that adding water to strong acids (pK_a < 8) results in an increase in the catalytic rate. As discussed, this is attributed to hydronium (or hydronium hydrate) formation in solution. In support of this statement, we find that the addition of water to anilinium (pK_a = 10.6) does not result in an increase in rate constant (Figure S31).

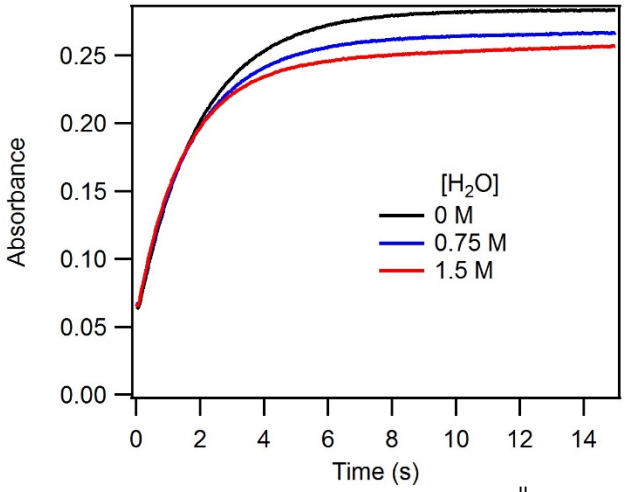

Figure S31. Stopped-flow kinetics traces for the reaction of $Ni^{II}H$ with 10 mM anilinium in the presence of H_2O to generate H_2 and Ni^{II}.

SI-7 Trifluoroacetic acid dimerization

Second Order Reactivity and Dimerization

It was reported in the literature than no dimerization is observed with trifluoroacetic acid in acetonitrile. Obtaining second order kinetics for the acids only has two possible explainations, either a termolecular reaction is occurring (i.e. Rate = $k[Ni^{II}H][AH]^2$) or the acid is dimerizing (i.e. Rate = $k[Ni^{II}H][(AH)_2]$) with a small enough dimerization constant such that $[(AH)_2] \propto [AH]^2$. We obtained an upper bound for the dimerization constant of 1 M^{-1} to see second order reactivity by determining that point at which $[(AH)_2] \propto [AH]^2$ no longer held true (Figure S32).

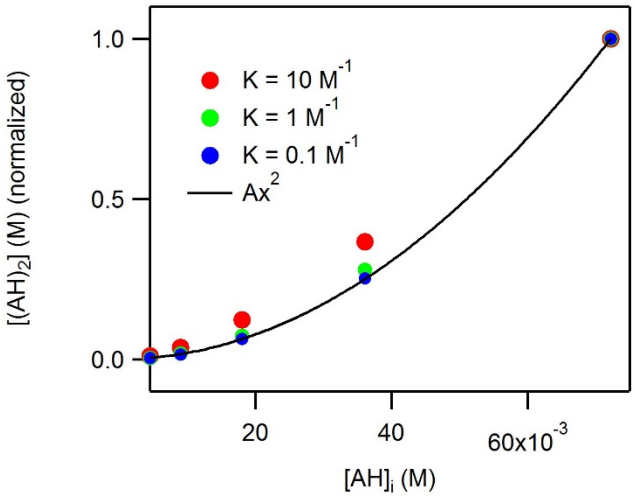

Figure S32. Expected concentration of $(AH)_2$, normalized to one at the highest input concentration of AH, $[AH]_I$, (chosen to match the concentrations in the trifluoroacetic acid experiment), given a dimerization constant of 10, 1, and 0.1 M^{-1}. The black line represents a true second order curve. At 1 M^{-1} we see a slight deviation from second order and anything higher than that would no longer give a satisfactory fit to second order kinetics, suggesting that if trifluoroacetic acid and trichloroacetic acid are dimerizing, the dimerization constant is below 1 M^{-1}.

References

(1) McCarthy, B. D.; Martin, D. J.; Rountree, E. S.; Ullman, A. C.; Dempsey, J. L. *Inorg. Chem.* **2014**, *53*, 8350–8361.

(2) Kaljurand, I.; Kütt, A.; Sooväli, L.; Rodima, T.; Mäemets, V.; Leito, I.; Koppel, I. A. *J. Org. Chem.* **2005**, *70*, 1019–1028.

(3) Rountree, E. S.; Dempsey, J. L. *J. Am. Chem. Soc.* **2015**, *137*, 13371–13380.

(4) Rountree, E. S.; Martin, D. J.; McCarthy, B. D.; Dempsey, J. L. *ACS Catalysis* **2016**. DOI: 10.1021/acscatal.6b00667.

(5) Hansch, C.; Leo, A.; Taft, R. W. *Chem. Rev.* **1991**, *91*, 165–195.

(6) Fulmer, G. R.; Miller, A. J. M.; Sherden, N. H.; Gottlieb, H. E.; Nudelman, A.; Stoltz, B. M.; Bercaw, J. E.; Goldberg, K. I. *Organometallics* **2010**, *29*, 2176–2179.